

RESEARCH

Open Access



# Morphological changes in flatfoot: a 3D analysis using weight-bearing CT scans

Yuchun Cai<sup>1†</sup>, Zhe Zhao<sup>2†</sup>, Jianzhang Huang<sup>1</sup>, Zhendong Yu<sup>3</sup>, Manqi Jiang<sup>1</sup>, Shengjie Kang<sup>4</sup>, Xinghong Yuan<sup>3</sup>, Yingying Liu<sup>3</sup>, Xiaoliu Wu<sup>5</sup>, Jun Ouyang<sup>6\*</sup>, Wencui Li<sup>2\*</sup> and Lei Qian<sup>7\*</sup>

## Abstract

**Background** Flatfoot is a condition resulting from complex three-dimensional (3D) morphological changes. Most previous studies have been constrained by using two-dimensional radiographs and non-weight-bearing conditions. The deformity in flatfoot is associated with the 3D morphology of the bone. These morphological changes affect the force line conduction of the hindfoot/midfoot/forefoot, leading to further morphological alterations. Given that a two-dimensional plane axis overlooks the 3D structural information, it is essential to measure the 3D model of the entire foot in conjunction with the definition under the standing position. This study aims to analyze the morphological changes in flatfoot using 3D measurements from weight-bearing CT (WBCT).

**Method** In this retrospective comparative our CT database was searched between 4–2021 and 3–2022. Following inclusion criteria were used: Patients were required to exhibit clinical symptoms suggestive of flatfoot, including painful swelling of the medial plantar area or abnormal gait, corroborated by clinical examination and confirmatory radiological findings on CT or MRI. Healthy participants were required to be free of any foot diseases or conditions affecting lower limb movement. After applying the exclusion criteria (Flatfoot with other foot diseases), CT scans (mean age = 20.9375, SD = 16.1) confirmed eligible for further analysis. The distance, angle in sagittal/transverse/coronal planes, and volume of the two groups were compared on reconstructed 3D models using the t-test. Logistic regression was used to identify flatfoot risk factors, which were then analyzed using receiver operating characteristic curves and nomogram.

**Result** The flatfoot group exhibited significantly lower values for calcaneofibular distance ( $p = 0.001$ ), sagittal and transverse calcaneal inclination angle ( $p < 0.001$ ), medial column height ( $p < 0.001$ ), sagittal talonavicular coverage angle ( $p < 0.001$ ), and sagittal ( $p < 0.001$ ) and transverse ( $p = 0.015$ ) Hibb angle. In contrast, the sagittal lateral talocalcaneal angle ( $p = 0.013$ ), sagittal ( $p < 0.001$ ) and transverse ( $p = 0.004$ ) talocalcaneal angle, transverse talonavicular coverage angle ( $p < 0.001$ ), coronal Hibb angle ( $p < 0.001$ ), and sagittal ( $p < 0.001$ ) and transverse ( $p = 0.001$ ) Meary's angle were significantly higher in the flatfoot group. The sagittal Hibb angle ( $B = -0.379$ ,  $OR = 0.684$ ) and medial column height ( $B = -0.990$ ,  $OR = 0.372$ ) were identified as significant risk factors for acquiring a flatfoot.

<sup>†</sup>Yuchun Cai and Zhe Zhao contributed equally to this work as co-first authors.

\*Correspondence:

Jun Ouyang

jouyang@126.com

Wencui Li

liwencui595@163.com

Lei Qian

dorisql712@126.com

Full list of author information is available at the end of the article



**Conclusion** The findings validate the 3D spatial position alterations in flatfoot. These include the abduction of the forefoot and prolapse of the first metatarsal proximal, the arch collapsed, subluxation of the talonavicular joint in the midfoot, adduction and valgus of the calcaneus, adduction and plantar ward movement of the talus in the hindfoot, along with the first metatarsal's abduction and dorsiflexion in the forefoot.

**Keywords** Flatfoot, Deformity, Weight-bearing CT, Entire foot, 3D measurement

## Introduction

Flatfoot, a common condition characterized by the collapse of the foot arch [1], can be either congenital or acquired. In children, flexible flatfoot is often due to underdeveloped arches, while congenital flatfoot is attributed to adhesive tarsal bones and congenital vertical talus [2–5]. Acquired flatfoot arises when children with normal arches develop flatfoot during growth, primarily due to factors such as a tight gastrocnemius–soleus complex, obesity, posterior tibial tendon dysfunction, or weakened plantar fascia and other arch-supporting ligaments [6–10].

Previous studies have described the morphological changes in flatfoot using various parameters [11–15] (Table 1). These parameters, including the calcaneofibular and talofibular distances, calcaneal inclination (CIA), lateral talocalcaneal (LTCA), and talocalcaneal (TCA) angles, as well as the angle between the talus and calcaneus (TACA), are used to evaluate the relative spatial displacement of the hindfoot bones and fibula. The collapse of the midfoot can be assessed by medial column height (MCH), talonavicular coverage angle (TNCA), and sinus tarsi volume. The first metatarsal–calcaneal angle (Hibb angle) and the talar first metatarsal angle (Meary's angle) are measured in the forefoot to assess the relative space-displacement of the hindfoot and the first metatarsal bone. However, these parameters, used in most previous studies, are applicable for two-dimensional or simulated weight-bearing CT and do not reflect the three-dimensional morphology of the entire flatfoot under the standing loading condition.

Under physiological loading, the foot acts as a force conduction structure. The collapse of the medial longitudinal arch weakens the leverage effect of the midfoot and affects the force transmission from the hindfoot to the forefoot [16]. Therefore, it is necessary to measure the alignment of the entire foot under physiological weight-bearing conditions. The clinical diagnosis of flatfoot is often based on X-ray, which is limited to a certain plane. But the parameters of flatfoot changes in multiple planes, which can be better represented by 3D measurement without multiple measurements [17]. So 3D measurement can show the bones in the position of the three planes which can better evaluate the deformity of flatfoot [18].



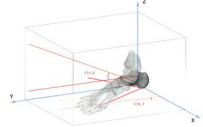
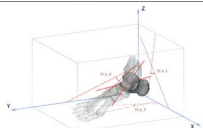
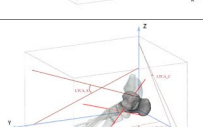
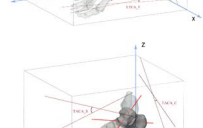
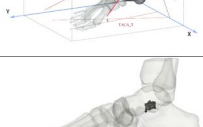


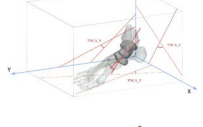
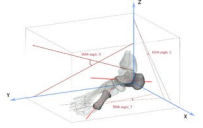
Most previous studies have used non-weight-bearing conditions or two-dimensional (2D) measurements using X-ray or CT data, which cannot explore the complex anatomical alignment of the foot. X-ray imaging cannot display three-dimensional (3D) foot bone structures due to bone overlap, projection positions, methodological differences, and limb rotation [19–21]. However, weight-bearing X-ray can show the alignment and structural stability of the foot under physiological standing conditions. Accurate evaluation of the alignment and rotation of the affected foot before an operation is crucial for treatment plans and prognosis. Routine clinical CT imaging, commonly performed with patients in the supine position, cannot objectively show the physiological load-bearing structures of the foot. Weight-bearing CT (WBCT) uses cone beam CT (CBCT) and natural weight bearing to evaluate lower extremity joints. CBCT uses a low dose of radiation, varying slightly between device manufacturers, and provides high-resolution images with sub-millimeter isotropic voxels [9, 22]. Therefore, WBCT provides a functional examination that can directly reflect the performance of the foot in the standing state and the subtle morphological changes in the relationships between bones and joints [23]. The objective of the present study was to explore the morphological alignment of the entire foot under the physiological standing loading of flatfoot using 3D reconstructions acquired from WBCT. With respect to this aim, our hypothesis is that the space position change of the flatfoot in the multiple planes can be clearly presented by 3D measurement under the WBCT.

## Materials and methods

### Study participants

The participants underwent CBCT scanning using a Verity scanner (Planmed Oy, Helsinki, Finland) at The Second People's Hospital of Shenzhen between April 28, 2021, and March 1, 2022. The study comprised 32 patients (Age:  $20.93 \pm 16.11$ , Weight:  $55.18 \pm 12.88$ , Length:  $157.64 \pm 8.7$ , BMI:  $22.04 \pm 27.12$ , 25 men, 7 women, 13 left feet, 19 right feet) and 30 healthy participants (Age:  $22.80 \pm 1.92$ , Weight:  $61.63 \pm 14.90$ , Length:  $165.3 \pm 7.61$ , BMI:  $22.35 \pm 4.57$ , 16 men, 14 women, 12 left feet, 18 right feet). Flatfoot in patients aged under 14 years is classified as developmental flatfoot. Consequently, patients were stratified based on their age at data

**Table 1** The measuring method and the image of flatfoot parameter

Name	Measurement method	Image
calcaneofibular distance	the line connecting the lowest point of the fibula to the lateral outburst of the calcaneus.	
talofibular distance	the line connecting the lowest point of the fibula to the lateral outburst of the talus.	
Hindfoot calcaneal inclination angle, CIA	the angle between the line connecting the most inferior points of calcaneal and the y axis.	
talocalcaneal angle, TCA	the angle between the line connecting the most lateral points of calcaneal and the long axis <sup>a</sup> of talus.	
lateral talocalcaneal angle, LTCA	the angle between the line connecting the most inferior points of calcaneal and the long axis of talus.	
TACA	the angle between the line connecting the talus and calcaneus.	
sinus tarsi volume	a tube or tunnel between the talus and the calcaneus bones and the two ends of the bottom surface of the talus, which is the upper dome of the sinus tarsi, were used as the boundary.	
Midfoot medial column height, MCH	The MCH is measured in the sagittal plane from the medial cuneiform to the line connecting the lowest point of the second metatarsal and calcaneus.	
talonavicular coverage angle, TNCA	the angle between the line connecting the long axes of talus and navicular.	
Forefoot first metatarsal-calcaneal angle, Hibb angle	the angle between the long axes of the calcaneal and the 1st metatarsal bone.	
talar first metatarsal angle, Meary's angle	the angle between the long axes of the talus and the 1st metatarsal bone.	

<sup>a</sup> The "long axis" of bone is generated by the automatic analysis of "mimics" according to the shape and structure of bone

collection. There were 12 patients younger than 14 years and 10 patients older than 14 years in the flatfoot group.

**Image acquisition and processing**

In the CT coordinate system, an anatomical reference system was defined with the z-axis orthogonal to the ground. For each foot, the lower leg was perpendicular to the floor and the line from most plantar vertex of the calcaneus to the center of the head of the second metatarsal bone is parallel to the Y-axis. All feet were realigned to this anatomical reference frame. Patients were required to exhibit clinical symptoms suggestive of flatfoot, including painful swelling of the medial plantar area or abnormal gait, corroborated by clinical examination and confirmatory radiological findings on CT or MRI. Healthy control group participants were required to be free of any foot diseases or conditions affecting lower limb movement. Axial planar images were obtained at a resolution of 801×801 pixels and a slice thickness of 0.2 mm. These images were then imported into Mimics 14.11 software (Materialise NV, Leuven, Belgium) to construct 3D foot models.

**Measured and calculated parameters**

Parameter measurements encompassed distance, angle, and volume. (Table 1) In the hindfoot, we measured and calculated: calcaneofibular distance, talofibular distance, CIA, LTCA, TACA, TCA and sinus tarsi volume; in the midfoot, we measured and calculated: MCH and TNCA; in the forefoot, we measured and calculated: Hibb\_angle and Meary's angle. Definition and measurement of all parameters are in Table 1.

These parameters were further divided into three parts according to the anatomical regions of the forefoot, midfoot, and hindfoot. All distance and angle parameters were measured using 3-Matic software (v13.0; Materialise NV). The 3D measurement data can be expressed by Euler Angle or quaternion, but both are more commonly used in basic research [24]. Therefore, we projected the 3D measurement data onto three planes, which is more convenient for clinical application. The angle measurements provided 3D angles projected in the coronal, sagittal, and transverse planes. The coronal plane was along the mediolateral axis (X–Z), the sagittal plane was along the longitudinal axis (Y–Z), and the transverse plane was along the dorsal–plantar anatomical direction (X–Y). For example, the CIA projected in the sagittal plane was defined as CIA\_S [25]. The model volumes were calculated automatically using the "properties" function after reconstruction of the sinus tarsi in Mimics software.

**Table 2** Comparison between the patients aged under 14 years and aged over 14 years in flatfoot group

	Variable	Anatomical plane	Mann–Whitney U/Two independent-sample t -test	p Value
Hindfoot	calcaneofibular distance	---	100	0.454
	talofibular distance	---	87	0.209
	CIA	S	0.805	0.427
		T	0.960	0.345
	LTCA	C	99	0.431
		S	77	0.099
		T	112	0.774
	TACA	C	108	0.659
		S	47	0.004*
		T	100	0.454
TCA	C	89	0.239	
	S	-0.760	0.453	
	T	1.930	0.063	
	Sinus tarsi volume	---	109.00	0.687
Midfoot	MCH	S	-1.802	0.082
	TNCA	C	-0.384	0.703
		S	-1.693	0.101
		T	1.170	0.251
Forefoot	Hibb angle	C	0.548	0.587
		S	1.077	0.290
		T	1.422	0.165
	Meary's angle	C	-0.932	0.359
		S	1.148	0.260
		T	108	0.659

CI confidence interval, CIA Calcaneal inclination angle, LTCA lateral talocalcaneal angle, TACA angle between the talus and calcaneus, TCA talocalcaneal angle, MCH medial column height, TNCA talonavicular coverage angle, Hibb angle first metatarsal–calcaneal angle, Meary's angle talar first metatarsal angle, C coronal, S sagittal, T transverse, SD standard deviation

\* Denotes a significant difference (\* $p < 0.05$ , \*\* $p < 0.001$ ) between the healthy group and flatfoot group

### Statistical analyses

There is age difference in the flatfoot group (20 patients were under 14 years old, and 10 patients were over 14 years old). In order to integrate them, we conducted Shapiro–Wilk Test on the data of patients under the age of 14 and over the age of 14 in the flatfoot group, and the Mann–Whitney U test provided  $U$  values and  $p$  values (threshold:  $p < 0.05$ ) was conducted on the data that did not meet the normal distribution. The  $t$  test provided  $t$  values and  $p$  values (threshold:  $p < 0.05$ ) was conducted on the data conforming to the normal distribution, and the results are shown in Table 2. Descriptive data are presented as mean  $\pm$  standard deviation and 95% confidence intervals (CIs). Differences between the flatfoot and control groups were analyzed using two-sample independent samples  $t$ -tests, with  $t$  values and  $p$  values provided. Logistic regression analysis was utilized to

explore the factors related to flatfoot, with odds ratios (ORs) and  $B$  values provided. ORs are an exact estimate of relative risk. An OR value greater than 1 indicated that the analyzed factor was a risk factor for flatfoot. OR values less than 1 indicated that the analyzed factor was a protective factor. OR values equal to 1 indicated that the factor played no role in the occurrence of the disease. Receiver operating characteristic (ROC) curves were used to analyze the sensitivity and specificity of all parameters. SPSS statistical software (v20.0; IBM Corp., Armonk, NY, USA) was used for statistical analysis.  $P$  values  $< 0.05$  were considered statistically significant. Nomograms were created based on a multivariate regression analysis, integrating multiple predictors, and then drawing line segments with certain proportions on the same plane to express the relationships between the variables in the prediction model.

**Table 3** 95%CI, Mean  $\pm$  SD and *p*- values of flatfoot parameters

position	Variable	Anatomical plane	Control Group ( <i>n</i> = 30)		Flatfoot Group ( <i>n</i> = 32)		<i>p</i> value
			Mean $\pm$ SD	95% CI	Mean $\pm$ SD	95% CI	
Hindfoot	calcaneofibular distance	—	6.37 $\pm$ 1.90	5.66–7.08	4.83 $\pm$ 1.49	4.29–5.36	0.001*
	talofibular distance	—	6.08 $\pm$ 2.07	5.31–6.85	6.09 $\pm$ 2.03	5.35–6.82	0.992
	CIA	S	20.20 $\pm$ 3.70	18.82–21.58	11.89 $\pm$ 3.95	10.46–13.31	< 0.001**
		T	16.50 $\pm$ 4.49	14.82–18.17	9.94 $\pm$ 4.32	8.38–11.49	< 0.001**
	LTCA	C	22.11 $\pm$ 13.88	18.82–21.58	22.57 $\pm$ 20.79	10.46–13.31	0.919
		S	34.83 $\pm$ 4.58	18.82–21.58	39.33 $\pm$ 8.57	10.46–13.31	0.013*
		T	42.23 $\pm$ 6.15	14.82–18.17	41.81 $\pm$ 9.83	8.38–11.49	0.845
	TACA	C	45.50 $\pm$ 18.87	38.45–52.54	55.98 $\pm$ 30.96	44.82–67.14	0.116
		T	30.84 $\pm$ 6.20	28.52–33.15	31.28 $\pm$ 8.09	28.36–34.20	0.809
	TCA	C	51.38 $\pm$ 27.56	41.09–61.67	54.47 $\pm$ 27.42	44.59–64.36	0.659
S		18.42 $\pm$ 11.49	14.13–22.71	34.25 $\pm$ 8.76	34.25–31.09	< 0.001**	
T		22.23 $\pm$ 5.45	20.19–24.26	26.97 $\pm$ 7.02	24.44–29.51	0.004*	
	Sinus tarsi volume	—	866.46 $\pm$ 207.43	789.00–943.91	801.53 $\pm$ 251.80	710.75–892.32	0.274
Midfoot	MCH	S	18.08 $\pm$ 3.26	16.86–19.30	8.84 $\pm$ 3.64	7.53–10.15	< 0.001**
	TNCA	C	76.97 $\pm$ 11.16	72.80–81.13	71.75 $\pm$ 10.53	67.95–75.55	0.064
		S	23.51 $\pm$ 7.01	20.89–26.13	11.51 $\pm$ 7.85	8.68–14.35	< 0.001**
	T	39.28 $\pm$ 11.30	35.06–43.50	50.78 $\pm$ 10.50	47.00–54.57	< 0.001**	
Forefoot	Hibb angle	C	17.48 $\pm$ 13.29	12.52–22.44	42.64 $\pm$ 26.73	33.00–52.27	< 0.001**
		S	36.49 $\pm$ 5.37	34.49–38.49	16.86 $\pm$ 9.88	13.30–20.43	< 0.001**
		T	17.16 $\pm$ 6.84	14.61–19.72	12.40 $\pm$ 8.03	9.50–15.29	0.015*
	Meary's angle	C	31.96 $\pm$ 15.15	26.31–37.62	27.13 $\pm$ 20.69	19.67–34.59	0.301
		S	6.37 $\pm$ 3.66	5.00–7.73	21.50 $\pm$ 11.61	21.50–26.69	< 0.001**
		T	14.58 $\pm$ 9.68	10.97–18.19	24.59 $\pm$ 12.06	20.24–28.94	0.001*

CI confidence interval, CIA Calcaneal inclination angle, LTCA lateral talocalcaneal angle, TACA angle between the talus and calcaneus, TCA talocalcaneal angle, MCH medial column height, TNCA talonavicular coverage angle, Hibb angle first metatarsal–calcaneal angle, Meary's angle talar first metatarsal angle, C coronal, S sagittal, T transverse, SD standard deviation

\* Denotes a significant difference ( $p < 0.05$ ,  $**p < 0.001$ ) between the healthy group and flatfoot group

## Results

In this study, there was no difference between the left and right feet of the sample using a two-sample t-test. The Mann–Whitney U test showed a significant difference in TACA\_S between the flatfoot groups aged under and over 14 years ( $p = 0.004$ ), while the other parameters were not statistically significant [26] (Table 2). The descriptive parameters of the feet with flatfoot and healthy control groups are shown in Table 3 and Fig. 1. For the hindfoot, calcaneofibular distance ( $p = 0.001$ , Fig. 2), CIA\_S ( $p < 0.001$ , Fig. 3a), and CIA\_T ( $p < 0.001$ , Fig. 3b)

in the flatfoot group were significantly lower than those in the control group. TCA\_S ( $p < 0.001$ , Fig. 4a), TCA\_T ( $p = 0.004$ , Fig. 4b), and LTCA\_S ( $p = 0.013$ , Fig. 5) were significantly larger in the flatfoot group than in the control group. For the midfoot, MCH ( $p < 0.001$ , Fig. 6) and TNCA\_S ( $p < 0.001$ , Fig. 7a) were significantly lower in the flatfoot group than in the control group. TNCA\_T ( $p < 0.001$ , Fig. 7b) was significantly larger in the flatfoot group than in the control group. For the forefoot, Hibb angle\_S ( $p < 0.001$ , Fig. 8b) and Hibb angle\_T ( $p = 0.015$ , Fig. 8c) were significantly smaller in the flatfoot group

(See figure on next page.)

**Fig. 1** Graph showing the mean parameters measured in the control group and flatfoot group. Hindfoot parameters included the calcaneofibular distance, talofibular distance calcaneal inclination angle (CIA), lateral talocalcaneal angle (LTCA), angle between the talus and calcaneus (TACA), talocalcaneal angle (TCA), and sinus tarsi volume. Midfoot parameters included the medial column height (MCH) and talonavicular coverage angle (TNCA). Forefoot parameters included the first metatarsal–calcaneal angle (Hibb angle) and talar first metatarsal angle (Meary's angle). Error bars represent one standard deviation above and below the mean. \*Denotes a significant difference ( $p < 0.05$ ,  $**p < 0.001$ ) between the control group and flatfoot group

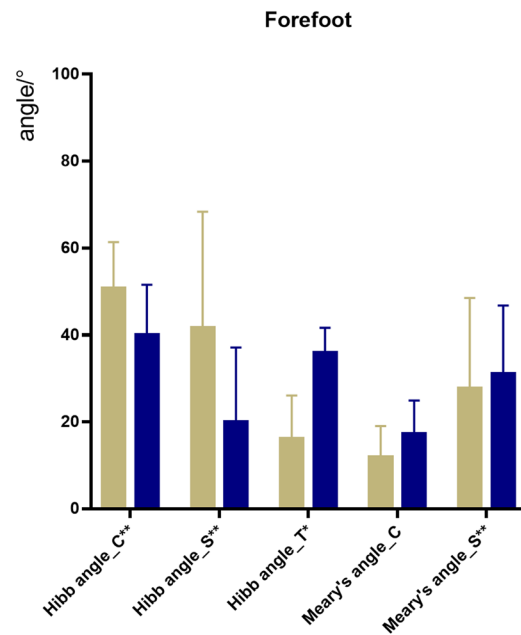
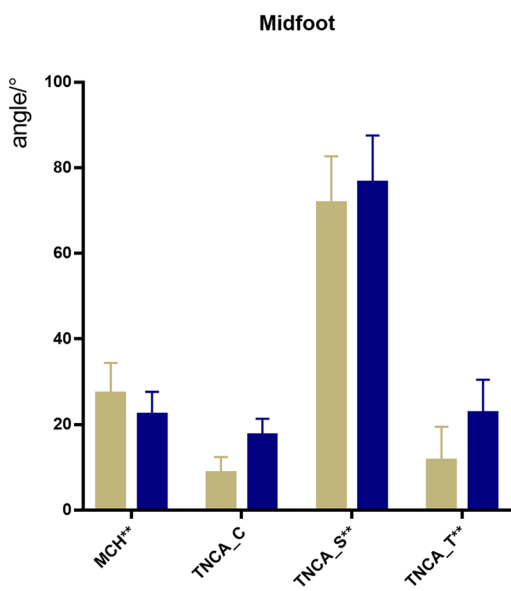
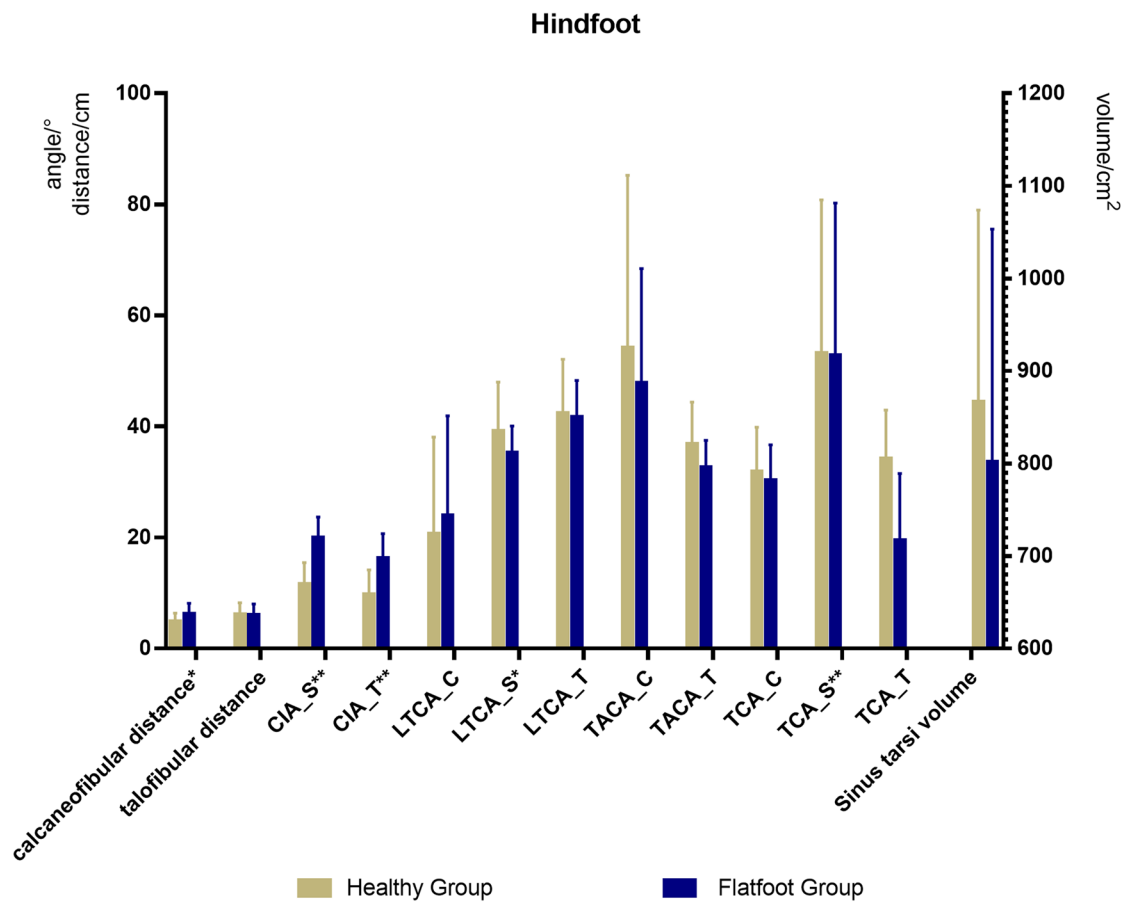
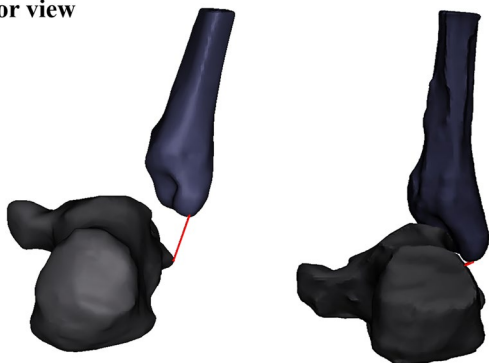


**Fig. 1** (See legend on previous page.)

Posterior view

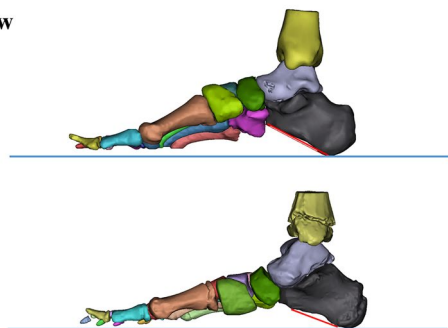


calcaneofibular distance

**Fig. 2** Calcaneofibular distance in a foot with flatfoot group (right) in a standing position showed significantly reduced distance compared to healthy control group (left)

**a**

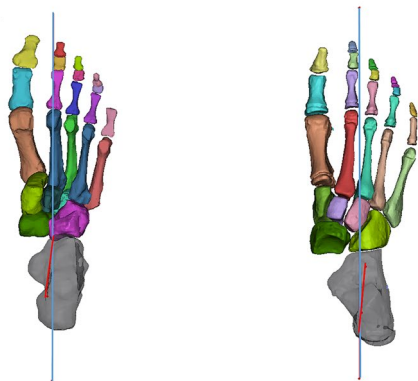
Lateral view



CIA\_S

**b**

Superior view

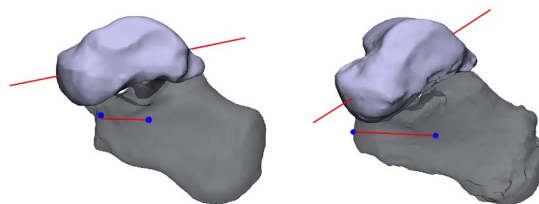


CIA\_T

**Fig. 3** **a** shows that the calcaneal inclination angle (CIA) of the flatfoot group (below) was significantly reduced compared with the control group (above) in the lateral view, and **b** shows that the CIA of the flatfoot group (right) was significantly reduced compared with the control group (left) in the superior view

**a**

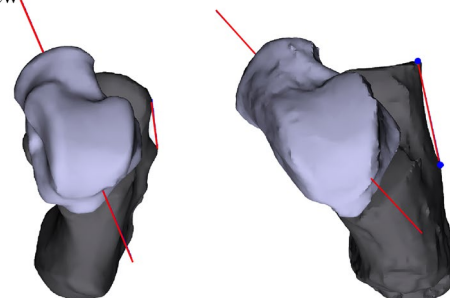
Lateral view



TCA\_S

**b**

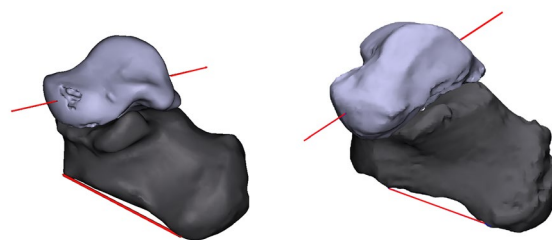
Superior view



TCA\_T

**Fig. 4** The talocalcaneal angle (TCA) in a foot with flatfoot group (right) in a standing position showed a significant increase in the lateral (Fig. 4a) and superior (Fig. 4b) views compared with the control group (left)

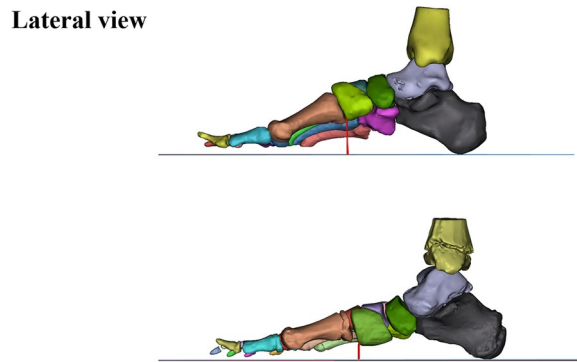
Lateral view



LTCA\_S

**Fig. 5** The lateral talocalcaneal angle (LTCA) in a foot with flatfoot group (right) in a standing position showed a significant increase in the lateral view compared with the control group (left)

than in the control group. Meary's angle\_S ( $p < 0.001$ , Fig. 9a), Meary's angle\_T ( $p = 0.001$ , Fig. 9b), and Hibb angle\_C ( $p < 0.001$ , Fig. 8a) were significantly larger in the flatfoot group than in the control group. Logistic regression revealed the risk prediction model of the occurrence of flatfoot by selecting statistically significant risk factors and using a forward stepwise regression procedure. In this model, statistically significant factors were Hibb angle\_S ( $B = -0.379$ ,  $OR = 0.684$ ) and MCH



**MCH**

**Fig. 6** The medial column height (MCH) in a foot with flatfoot group (below) in a standing position showed a significant reduction in the lateral view compared with the control group (above)

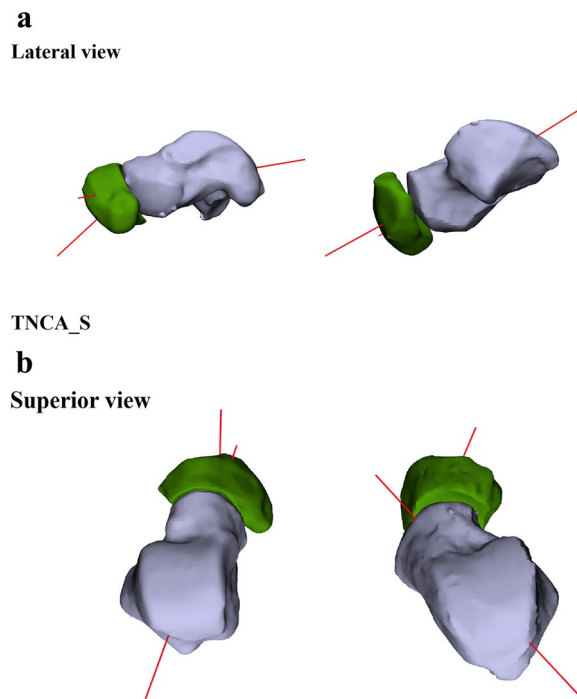


**Fig. 7** The talonavicular coverage angle (TNCA) in a foot with flatfoot group (right) in a standing position showed a significant reduction in the lateral and increase in the superior views compared with the control group (left)

( $B = -0.990$ ,  $OR = 0.372$ ). The area under the ROC curve of Hibb angle\_S and MCH were 0.962 (95% CI: 0.917–1) and 0.976 (95% CI: 0.946–1), and the cut-off values were 0.844 and 0.87, respectively (Fig. 10). The nomogram demonstrated the comprehensive effects of these two sensitivity factors on flatfoot, and the two parameters

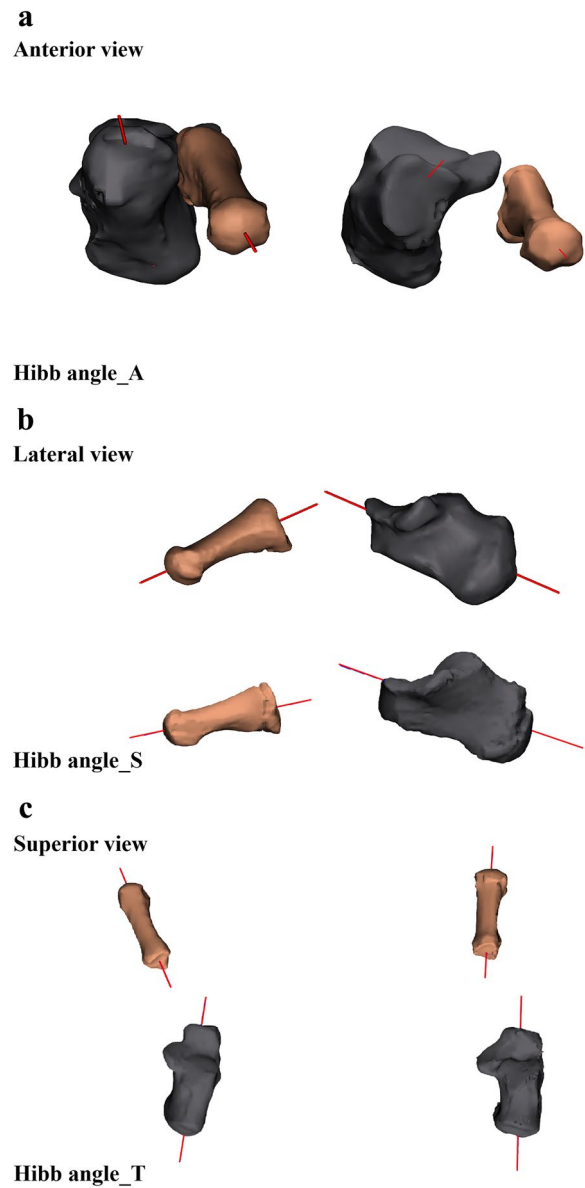


**Fig. 8 a** The first metatarsal–calcaneal angle (Hibb angle) in a foot with flatfoot group (right) in a standing position showed a significant increase in the anterior view compared with the control group (left). **b** The Hibb angle in a foot with flatfoot group (below) showed a significant reduction in the anterior view compared with the control group (above). **c** The Hibb angle in a foot with flatfoot group (right) showed a significant reduction in the superior view compared with the control group (left)

were negatively correlated with the occurrence of flatfoot (Fig. 11).

**Discussion**

In this study, we compared 3D parameters between flat-foot and healthy control groups using WBCT data. The results revealed deformations in the forefoot, midfoot,



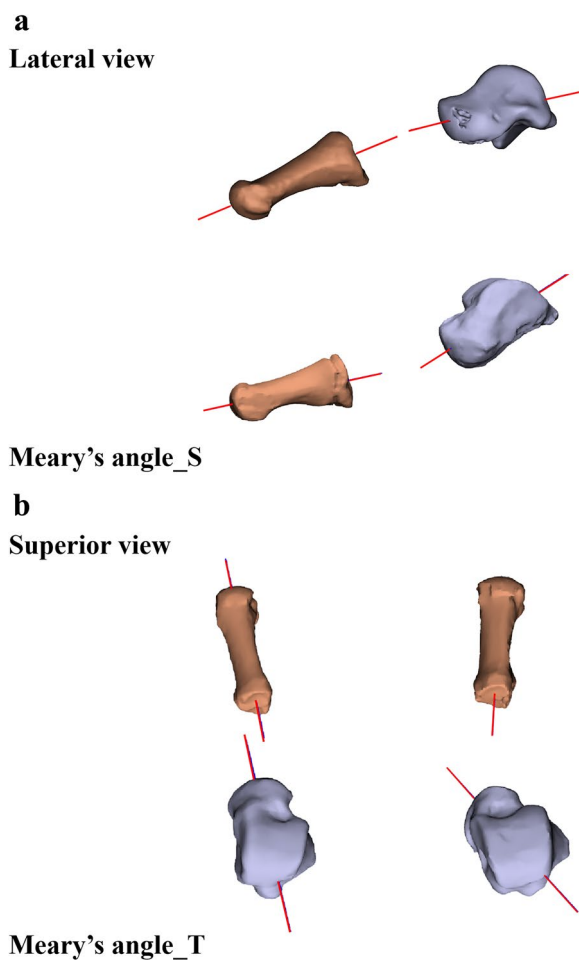


**Fig. 9** **a** The talar first metatarsal angle (Meary's angle) in a foot with flatfoot group (below) in a standing position showed a significant increase in the lateral view compared with the control group (above). **b** The Meary's angle in a foot with flatfoot group (right) showed a significant increase in the superior view compared with the control group (left)

and hindfoot. This is consistent with previous studies that identified the morphological features of flatfoot as the collapse of the medial longitudinal arch, heel valgus deformity, and forefoot abduction [15].

Broos et al. [27] proposed based on experiment that little qualitative difference between 2 and 3D measurements, albeit with slight quantitative differences. However, the variation in 3D parameters was generally smaller than those in the 2D parameters, leading to the conclusion that the results of the 3D measurements were more accurate. Before the fully automated 3D measurement, many researchers often used weight-bearing radiographs or WBCT to generate 3D isosurfaces of bones, and used the rendered images to generate mathematical models to calculate the landmark positions and principal axes of bones [28, 29]. Even though all measurements were calculated automatically, the bone structure still needed manual selection. Ide Van den Borre [30] used WBCT for automatic cutting and bone segmentation and automatic measurement, and evaluation of foot and ankle alignment, avoid artificial measurement error, and provide clinical accurate measurement results.

In our study, WBCT data were examined with participants in a standing position. A study by Barg [31] demonstrated that traditional load-bearing radiograph was susceptible to technical errors, such as rotational misalignment, resulting in inaccurate measurements of pathological deformities. A study by Kido et al. [32] reported differences in talus, scaphoid, and calcaneus positions on WBCT data compared with non-weight-bearing CT data. WBCT has been used to quantify the severity of the Progressive Collapsing Foot Deformity (PCFD) with good intra- and interobserver reliability. [33, 34] Conti and Ellis [23] proposed that WBCT could better show the true orientation of bones and joints during loading compared with standard CT. Although Conti and Ellis [23] used a conventional CT scanner with an axial loading

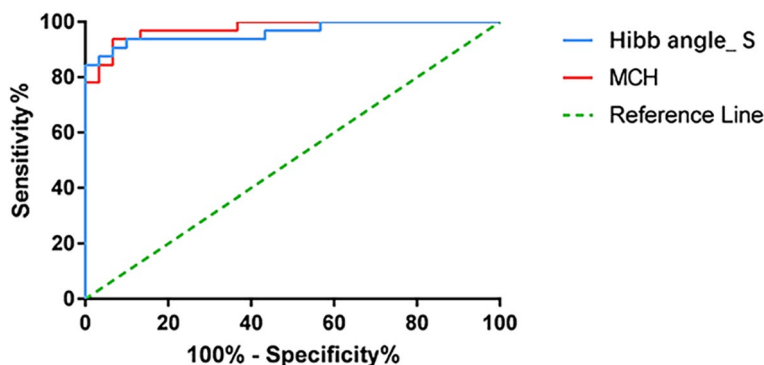


**Fig. 10** Receiver operating characteristic (ROC) curve of the determining parameters of flatfoot. Hibb Angle between the long axis of the calcaneal and the long axis of the first metatarsal bone. Medial column height (MCH) is the perpendicular distance between the most inferior aspect of the cuboid and a horizontal line through the tuberosity of the calcaneus. Hibb angle\_S and MCH showed an area under the ROC curve of 0.962 and 0.976 and cut-off values of 0.844 and 0.87, respectively

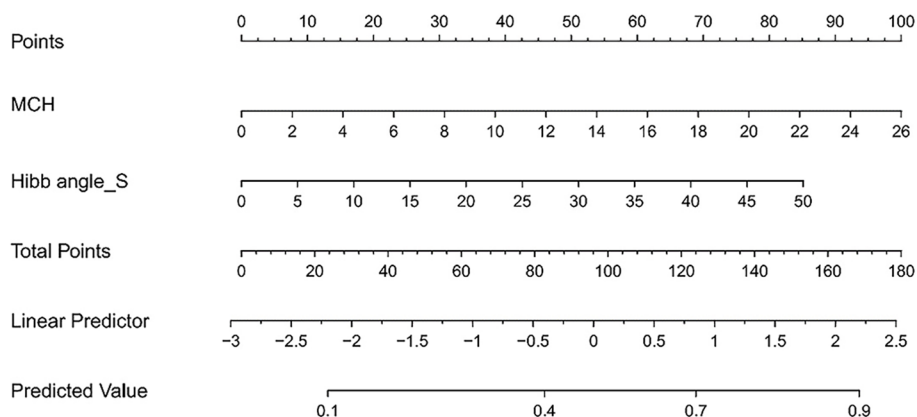


**Fig. 11** Logistic regression nomogram of parameters related to flatfoot occurrence. To use the nomogram, the values of MCH and Hibb angle\_S of individual patients are located on each variable axis. Dots are drawn upward to determine the points received by each variable. The sum of these points is located on the Total Points axis, and a line is drawn downward to the Predicted Value axis to determine the probability of flatfoot

device, such device are still not fully load-bearing and do not totally represent the features of a foot in a standing position.

**In the hindfoot**

As the arch collapses, the foot’s force conduction disorder causes spatial displacement of the calcaneus and talus in the hindfoot. The primary hindfoot differences in this study indicated a decreased calcaneofibular impingement rate, calcaneal adduction and eversion, and talus adduction and plantar flexion in the flatfoot group compared to the healthy group. The calcaneofibular distance, which assesses subfibular impingement, was significantly smaller in the flatfoot group compared with the control group, potentially related to adduction or valgus of the calcaneus [35]. Jeng et al. [36] performed WBCT in 25 patients with PCFD to assess subtalar and calcaneofibular impingement, finding that only 35% of patients had calcaneofibular impingement. The mean coronal calcaneofibular distance was 2.7 mm in patients with calcaneofibular impingement, compared with 5.7 mm in patients without calcaneofibular impingement. The CIA and TCA, both used to describe the alignment of the hindfoot, indicated a flatter foot with a lower CIA and a greater TCA [35]. Consistent with other studies [37, 38], we found the CIA\_S to be significantly smaller in the flatfoot group compared with the control group, indicating a decreased height of the medial longitudinal arch. Additionally, the CIA\_T was significantly smaller in the flatfoot group than in the control group, which may be due to increased calcaneal adduction or valgus. In this study, the TCA\_S and TCA\_T were significantly larger in the flatfoot group compared with the control group. Lo et al. [38] found that a flatfoot group had a significantly higher talus angle than a control group. The talus angle

provides an indication of talar inclination. Chen et al. [39] proposed that adduction and movement of the talus in the plantar direction become increasingly positive in individuals with flatfoot. Moreover, there was an increase in adduction or valgus of the calcaneus [40]. The LTCA is used in the assessment of subtalar joint valgus. In this study, the LTCA on the sagittal plane in the flatfoot group was significantly larger than that in the control group. According to Thapa et al., the LTCA increases with hindfoot valgus in the anteroposterior projection [41].

**In the midfoot**

The collapse of the midfoot is the initial factor in the pathogenesis of flatfoot, affecting the three-dimensional force transmission of the entire foot. The main midfoot difference indicated decreased medial arch height, talonavicular joint subluxation, and scaphoid abduction in the flatfoot group compared to the healthy group. The severity of medial arch collapse can be assessed using the MCH [15]. In this study, the MCH of the flatfoot group was significantly smaller than that of the control group. This decrease in MCH reflected increased collapse of the midfoot. The TNCA on the anteroposterior radiographs, known as Kite’s angle, reflects the degree of talar uncoverage [15]. The more severe the flatfoot deformity—or, in other words, the increase in the angle—the more uncovered the distal articular aspect of the talus is by the navicular [14]. In this study, TNCA\_S was significantly smaller in the flatfoot group than in the control group. TNCA\_T was significantly larger in the flatfoot group than in the control group. Zhang et al. [42] 3D measurement techniques to compare changes in the relative spatial position of the talonavicular joints (compared with healthy feet) in patients with stage II posterior tibial tendon dysfunction in non-weight-bearing and weight-bearing conditions.

In the talar joint, at 3° valgus of the talonavicular joint, the scaphoid shifted 1.3 mm outward, 0.8 mm forward, and 0.8 mm upward relative to the talus. This indicated that flatfoot involves a subluxation of the talonavicular joint and that this midfoot deformity may be affected by scaphoid abduction [43].

#### In the forefoot

To adapt to the collapse of the medial arch [16], the primary forefoot differences in the flatfoot group, compared to the healthy group, indicated abduction in the transverse plane and prolapse of the first metatarsal proximal in the sagittal plane. The Hibb angle, which is the angle between the axis of the calcaneus and the axis of the first metatarsal, was significantly smaller in the flatfoot group than in the control group. Previous studies have often shown that flatfoot involves forefoot supination and hindfoot abduction and external rotation on the anteroposterior view and dorsiflexion on the lateral view [44]. These changes lead to an increase in Meary's angle\_S and Meary's angle\_T and a decrease in the Hibb angle. Furthermore, our study found that the Hibb angle in the coronal plane was larger in the flatfoot group than in the control group. The talar first metatarsal angle, also known as Meary's angle, is defined as the angle between the long axis of the talus and the long axis of the first metatarsal bone [15, 45]. The lateral Meary's angle can reflect increased talar inclination and hindfoot pronation [35]. Our results showed that Meary's angle\_S and Meary's angle\_T were significantly larger in the flatfoot group than in the control group. Kido et al. [46] also reported that the rotation of the first metatarsal bone relative to the first tarsometatarsal joint under load was more dorsiflexed in flatfoot than in control foot.

In our study, the MCH and Hibb angle\_S were highly sensitive parameters for flatfoot. Similar to the study by Kang et al. [12], the mean MCH in our study was 8.84 mm for the flatfoot group and 18.08 mm for the control group, showing a significant difference. The occurrence of flatfoot was closely related to the MCH value. According to the ROC curve analysis, when the cut-off value was lower than 0.87 mm, the risk of arch collapse was significantly increased, and flatfoot was more likely. The Hibb Angle\_S showed high sensitivity in the diagnosis of flatfoot. A lower Hibb Angle\_S increased the incidence of forefoot and hindfoot collapse. Monitoring changes in Hibb angle\_S could have important clinical implications for reducing adverse outcomes in patients with flatfoot [21]. The nomogram intuitively reflected the effects of MCH and Hibb angle\_S on the occurrence of flatfoot. The addition of MCH and Hibb angle\_S scores in the nomogram directly corresponded to the occurrence of flatfoot, which could be helpful for the diagnosis

and severity assessment of flatfoot. There were some limitations to our study. First, as this study used WBCT, which was acquired using CBCT, the high consumption of CBCT resulted in low willingness of participants to undergo CBCT examination, limiting the sample size of each group. Second, this study did not consider degenerative changes due to advancing age. Overall, the results of this study need to be confirmed in future clinical studies.

#### Conclusion

Under the standing loading condition, this study analyzed the deformity of the entire foot in flatfoot using 3D measurements of WBCT data. The morphological changes in flatfoot can be succinctly summarized as midfoot collapse, hindfoot valgus, and forefoot abduction. Our study confirmed in detail the 3D spatial position changes in flatfoot, including abduction of the forefoot and prolapse of the first metatarsal proximal, decreased medial arch height, subluxation of the talonavicular joint in the midfoot, adduction and valgus of the calcaneus, adduction and plantar ward movement of the talus in the hindfoot, and the first metatarsal abduction and dorsiflexion in the forefoot. As demonstrated in this study, flatfoot involves more complex 3D spatial position changes. WBCT can reflect the performance of the foot in a standing state, and the use of 3D measurement parameters can reveal the subtle morphological changes of bone and joint correspondence. This provides more accurate information for the treatment planning of flatfoot.

#### Abbreviations

3D	Three-dimensional
WBCT	Weight-bearing CT
C	Coronal
S	Sagittal
T	Transverse
CIA	Calcaneal inclination angle
LTCA	Lateral talocalcaneal angle
TCA	Talocalcaneal angle
TACA	The talus and calcaneus angle
MCH	Medial column height
TNCA	Talonavicular coverage angle
2D	Two-dimensional

#### Supplementary Information

The online version contains supplementary material available at <https://doi.org/10.1186/s12880-024-01396-0>.

Supplementary Material 1.

#### Acknowledgements

Not applicable.

#### Authors' contributions

L.Q., Z.Z., X.I.W., and J.Oy. contributed to the conception of the study. Wc.L. performed the collection of sample CT images. Zd.Y., S.J.K., Xh.Y. and Yy.L. performed the Model reconstruction. Jz.H. contributed the Model measurement. Mq.J. performed the data analyses and data presentation. Yc.C. contributed significantly to the manuscript writing and the drawing of chart.

## Funding

This work was supported by the College Students' Innovative Entrepreneurial Training Plan Program (202212121002), and Basic and Applied Basic Research Project in Guangzhou (SL2023A04J01973), Guangdong, China.

## Availability of data and materials

The datasets used and analyzed during the current study are available from the corresponding author on reasonable request.

## Declarations

### Ethics approval and consent to participate

The experimental design was approved by our Institutional Review Board (Southern medical university ethics committee) before the study started, and the Ethical Committee Approval was submitted. The informed consent was obtained from all adult participants and minor participants' legal guardians in this experiment.

### Consent for publication

Not applicable.

### Competing interests

The authors declare no competing interests.

### Author details

<sup>1</sup>The Second School of Clinical Medicine, Southern Medical University, Guangzhou 510515, Guangdong, China. <sup>2</sup>Hand and Foot Surgery Department, The First Affiliated Hospital of Shenzhen University, Shenzhen Second People's Hospital, Shenzhen, Guangdong 518035, People's Republic of China. <sup>3</sup>The First School of Clinical Medicine, Southern Medical University, Guangzhou 510515, Guangdong, China. <sup>4</sup>School of Basic Medical Sciences, Southern Medical University, Guangzhou, Guangdong, China. <sup>5</sup>Radiologic Department, The First Affiliated Hospital of Shenzhen University, Shenzhen Second People's Hospital, Shenzhen, Guangdong 518035, People's Republic of China. <sup>6</sup>Guangdong Provincial Key Laboratory of Digital Medicine and Biomechanics and Guangdong Engineering Research Center for Translation of Medical 3D Printing Application and National Virtual and Reality Experimental Education Center for Medical Morphology (Southern Medical University) and National Experimental Education Demonstration Center for Basic Medical Sciences (Southern Medical University) and National Key Discipline of Human Anatomy, Department of Spine Surgery, Guangdong Provincial People's Hospital (Guangdong Academy of Medical Sciences), School of Basic Medical Sciences, Southern Medical University, Guangzhou, Guangdong, China. <sup>7</sup>Guangdong Provincial Key Laboratory of Digital Medicine and Biomechanics and Guangdong Engineering Research Center for Translation of Medical 3D Printing Application and National Virtual & Reality Experimental Education Center for Medical Morphology (Southern Medical University) and National Experimental Education Demonstration Center for Basic Medical Sciences (Southern Medical University) and National Key Discipline of Human Anatomy, School of Basic Medical Sciences, Southern Medical University, Guangzhou, Guangdong, China.

Received: 19 March 2024 Accepted: 7 August 2024

Published online: 19 August 2024

## References

- Smith MA. Flat feet in children. *BMJ*. 1990;301:942–3.
- Haveson SB. Congenital Flatfoot Due to Talonavicular Dislocation (Vertical Talus). *Radiology*. 1959;72:19–25.
- Shrimpton AE, Levinsohn EM, Yozawitz JM, Packard DS Jr, Cady RB, Middleton FA, et al. A HOX gene mutation in a family with isolated congenital vertical talus and Charcot-Marie-Tooth Disease. *Am J Hum Genet*. 2004;75:92–6.
- Golshteyn G, Schneider HP. Tarsal Coalitions. *Clin Podiatr Med Surg*. 2022;39:129–42.
- Arain A, Harrington MC, Rosenbaum AJ. Adult-Acquired Flatfoot. Treasure Island (FL): StatPearls Publishing; 2023.
- Abousayed MM, Alley MC, Shakked R, Rosenbaum AJ. Adult-acquired flatfoot deformity. *JBJS Reviews*. 2017;5:e7.
- Malden S, Gillespie J, Hughes A, Gibson A, Farooq A, Martin A, et al. Obesity in young children and its relationship with diagnosis of asthma, vitamin D deficiency, iron deficiency, specific allergies and flat-footedness: A systematic review and meta-analysis. *Obes Rev*. 2020;22(3):e13129.
- Tang CYK, Ng KH, Lai J. Adult flatfoot. *BMJ*. 2020;24(368):m295.
- Brinch S, Wellenberg RHH, Boesen M, Maas M, Elkjær Johannsen F, Damm Nybing J, et al. Weight-bearing cone-beam CT: the need for standardised acquisition protocols and measurements to fulfill high expectations—a review of the literature. *Skeletal Radiol*. 2022;52:1073–88.
- Rhim HC, Dhawan R, Gureck AE, Lieberman DE, Nolan DC, Elshafey R, et al. Characteristics and future direction of tibialis posterior tendinopathy research: a scoping review. *Medicina*. 2022;58:1858.
- Gentili A, Masih S, Yao L, Seeger LL. Foot axes and angles. *Br J Radiol*. 1996;69:968–74.
- Kang S-H, Charlton TP, Thordarson DB. Lateral column length in adult flatfoot deformity. *Foot Ankle Int*. 2013;34:392–7.
- Koca TT, Göğebakan H, Koçyiğit BF, Nacitarhan V, Yildir C.Z. Foot functions in ankylosing spondylitis. *Clin Rheumatol*. 2019;38:1083–8.
- Lau BC, Allahabadi S, Palanca A, Oji DE. Understanding radiographic measurements used in foot and ankle surgery. *J Am Acad Orthop Surgeons*. 2022;30:e139–54.
- Flores DV, Mejía Gómez C, Fernández Hernando M, Davis MA, Pathria MN. Adult acquired flatfoot deformity: anatomy, biomechanics, staging, and imaging findings. *Radiographics*. 2019;39:1437–60.
- Van Boerum DH, Sangeorzan BJ. Biomechanics and pathophysiology of flat foot. *Foot Ankle Clin*. 2003;8:419–30.
- Wagner E, Wagner P, Pacheco F, López M, Palma F, Guzmán-Venegas R, et al. biomechanical cadaveric evaluation of the role of medial column instability in hallux valgus deformity. *Foot Ankle Int*. 2022;43:830–9.
- Lintz F, de Cesar NC. Is advanced imaging a must in the assessment of progressive collapsing foot deformity? *Foot Ankle Clin*. 2021;26:427–42.
- Bock P, Pittermann M, Chraim M, Rois S. The inter- and intraobserver reliability for the radiological parameters of flatfoot, before and after surgery. *Bone Joint J*. 2018;100-B:596–602.
- Shakoor D, de Cesar NC, Thawait GK, Ellis SJ, Richter M, Schon LC, et al. Weight-bearing radiographs and cone-beam computed tomography examinations in adult acquired flatfoot deformity. *Foot Ankle Surg*. 2021;27:201–6.
- Meyr AJ, Wagoner MR. Descriptive quantitative analysis of rearfoot alignment radiographic parameters. *J Foot Ankle Surg*. 2015;54:860–71.
- Li J, Fang M, Van Oevelen A, Peiffer M, Audenaert E, Burssens A. Diagnostic applications and benefits of weightbearing CT in the foot and ankle: a systematic review of clinical studies. *Foot Ankle Surg*. 2024;30:7–20.
- Conti MS, Ellis SJ. Weight-bearing CT scans in foot and ankle surgery. *J Am Acad Orthop Surg*. 2020;28:e595–603.
- Burssens A, Peeters J, Peiffer M, Marien R, Lenaerts T, Vandeputte G, et al. Reliability and correlation analysis of computed methods to convert conventional 2D radiological hindfoot measurements to a 3D setting using weightbearing CT. *Int J Comput Assist Radiol Surg*. 2018;13:1999–2008.
- Orotolani M, Leardini A, Pavani C, Scicolone S, Girolami M, Bevoni R, et al. Angular and linear measurements of adult flexible flatfoot via weight-bearing CT scans and 3D bone reconstruction tools. *Sci Rep*. 2021;11(1):16139.
- Waseda A, Suda Y, Inokuchi S, Nishiwaki Y, Toyama Y. Standard growth of the foot arch in childhood and adolescence—Derived from the measurement results of 10,155 children. *Foot Ankle Surg*. 2014;20:208–14.
- Broos M, Berardo S, Dobbe JGG, Maas M, Streekstra GJ, Wellenberg RHH. Geometric 3D analyses of the foot and ankle using weight-bearing and non weight-bearing cone-beam CT images: The new standard? *Eur J Radiol*. 2021;138:109674.
- Kvarda P, Krähenbühl N, Susdorf R, Burssens A, Ruiz R, Barg A, et al. High reliability for semiautomated 3D measurements based on weightbearing CT scans. *Foot Ankle Int*. 2021;43:91–5.
- Krähenbühl N, Kvarda P, Susdorf R, Burssens A, Ruiz R, Barg A, et al. Assessment of progressive collapsing foot deformity using semiautomated 3D measurements derived from weightbearing CT scans. *Foot Ankle Int*. 2021;43:363–70.
- Van den Borre I, Peiffer M, Huysenruyt R, Huyghe M, Vervelghe J, Pizurica A, et al. Development and validation of a fully automated tool to quantify 3D foot and ankle alignment using weight-bearing CT. *Gait Posture*. 2024;113:67–74.

31. Barg A, Amendola RL, Henninger HB, Kapron AL, Saltzman CL, Anderson AE. Influence of ankle position and radiographic projection angle on measurement of supramalleolar alignment on the anteroposterior and hindfoot alignment views. *Foot Ankle Int.* 2015;36:1352–61.
32. Kido M, Ikoma K, Imai K, Tokunaga D, Inoue N, Kubo T. Load response of the medial longitudinal arch in patients with flatfoot deformity: in vivo 3D study. *Clin Biomech.* 2013;28:568–73.
33. de Cesar NC, Shakoor D, Dein EJ, Zhang H, Thawait GK, Richter M, et al. Influence of investigator experience on reliability of adult acquired flatfoot deformity measurements using weightbearing computed tomography. *Foot Ankle Surg.* 2019;25:495–502.
34. Barg A, Bailey TS, Richter M, Lintz F, Burssens A, et al. Weightbearing computed tomography of the foot and ankle: emerging technology topical review. *Foot Ankle Int.* 2018;39:376–86.
35. Frenkel Rutenberg T, Shemesh S, Rutenberg R, Heller S, Haviv B, Burg A. Lateral column lengthening for flexible flat foot: was it short to begin with? *Isr Med Assoc J.* 2021;23:506–9.
36. Jeng CL, Rutherford T, Hull MG, Cerrato RA, Campbell JT. Assessment of bony subfibular impingement in flatfoot patients using weight-bearing CT scans. *Foot Ankle Int.* 2018;40:152–8.
37. Younger AS, Sawatzky B, Dryden P. Radiographic assessment of adult flatfoot. *Foot Ankle Int.* 2005;26:820–5.
38. Lo H-C, Chu W-C, Wu W-K, Hsieh H, Chou C-P, Sun S-E, et al. Comparison of radiological measures for diagnosing flatfoot. *Acta Radiol.* 2012;53:192–6.
39. Chen C-H, Huang M-H, Chen T-W, Weng M-C, Lee C-L, Wang G-J. The correlation between selected measurements from footprint and radiograph of flatfoot. *Arch Phys Med Rehabil.* 2006;87:235–40.
40. Aronson J, Nunley J, Frankovitch K. Lateral talocalcaneal angle in assessment of subtalar valgus: follow-up of seventy Grice-Green arthrodeses. *Foot Ankle.* 1983;4:56–63.
41. Thapa MM, Pruthi S, Chew FS. Radiographic assessment of pediatric foot alignment: Review. *Am J Roentgenol.* 2010;194:S51–8.
42. Zhang Y, Xu J, Wang X, Huang J, Zhang C, Chen L, et al. An in vivo study of hindfoot 3D kinetics in stage II posterior tibial tendon dysfunction (PTTD) flatfoot based on weight-bearing CT scan. *Bone Joint Res.* 2013;2:255–63.
43. Seringe R, Wicart P, French Society of Pediatric Orthopaedics. The talonavicular and subtalar joints: the “calcaneopedal unit” concept. *Orthopaedics & traumatology, surgery & research: OTSR.* 2013;99(6 Suppl):S345–355.
44. Kadhim M, Holmes L, Miller F. Correlation of radiographic and pedobarograph measurements in planovalgus foot deformity. *Gait Posture.* 2012;36:177–81.
45. Lamm BM, Stasko PA, Gesheff MG, Bhav A. Normal foot and ankle radiographic angles, measurements, and reference points. *J Foot Ankle Surg.* 2016;55:991–8.
46. Kido M, Ikoma K, Imai K, Takatori R, Tokunaga D, et al. Load response of the tarsal bones in patients with flatfoot deformity: in vivo 3D study. *Foot Ankle Int.* 2011;32:1017–22.

## Publisher's Note

Springer Nature remains neutral with regard to jurisdictional claims in published maps and institutional affiliations.